Published in final edited form as:
Nat Chem Biol. 2017 May ; 13(5): 522–528. doi:10.1038/nchembio.2328.

The Rrp4-exosome complex recruits and channels substrate RNA by a unique mechanism

Milos A. Cvetkovic[1], **Jan Philip Wurm**[1], **Maxime J. Audin**[1], **Stefan Schütz**[1], and **Remco Sprangers**[1,*]

[1]Max Planck Institute for Developmental Biology, Spemannstrasse 35, 72076 Tübingen, Germany

Abstract

The exosome is a large molecular machine that is involved in RNA degradation and processing. Here, we address how the trimeric Rrp4 cap enhances the activity of the archaeal enzyme complex. Using methyl TROSY NMR methods we identified a 50 Å long RNA binding path on each Rrp4 protomer. We show that the Rrp4 cap can thus recruit three substrates simultaneously, one of which is degraded in the core while two others are positioned for subsequent degradation rounds. The local interaction energy between the substrate and the Rrp4-exosome increases from the periphery of the complex towards the active sites. Importantly, the intrinsic interaction strength between the cap and the substrate is weakened as soon as substrates enter the catalytic barrel, which provides a means to reduce friction during substrate movements towards the active sites. Our data thus reveal a sophisticated exosome–substrate interaction mechanism that enables efficient RNA degradation.

Introduction

The exosome is a large molecular machine that plays an essential role in RNA processing and degradation1–4. The archaeal and eukaryotic exosome share a common architecture and consist of a hexameric core and a trimeric cap structure. In eukaryotes, all subunits that constitute the core and the cap are unique proteins1. Despite this complexity, the 9-subunit eukaryotic exosome has lost the ability to degrade RNA on its own and requires an auxiliary subunit to perform this function5. In archaea, the exosome structure is simpler and has a three-fold symmetry (Fig. 1a)6–8. Its hexameric core is composed of three Rrp41-Rrp42 dimers, while the cap structure comprises a trimer of the Csl4 or Rrp4 proteins. In addition, the archaeal exosome is catalytically active, where the active sites are located within the

*Correspondence and requests for materials should be addressed to R.S. (remco.sprangers@tuebingen.mpg.de).

Author contributions
M.A.C. performed and analyzed NMR, binding and degradation experiments. J.P.W assisted with the binding experiments, M.J.A assisted with the degradation experiments, S.S. performed NMR assignment experiments. R.S. conceived the project and analyzed data. R.S wrote the manuscript, all authors commented on the data, the analysis and the manuscript.

Competing financial interests
The authors declare no competing financial interests.

Additional information
Reprints and permissions information is available online at http://www.nature.com/reprints/index.html.

Europe PMC Funders Author Manuscripts

Rrp41 subunits in the interior of the hexameric core. Multiple structures of eukaryotic9–11 and archaeal12–16 exosome complexes have been determined in recent years and these provide fundamental insights into the functioning of the enzyme.

The archaeal exosome structure displays an RNA entrance funnel. During catalytic degradation the RNA is progressively threaded from the outside into the hexameric barrel, where successive diphosphate nucleotides are removed from the 3’ end of the RNA substrate in a phosphorolytic manner13,17,18. The cap proteins feature conserved S1, KH and Zn-ribbon RNA binding domains6. The S1 domains of the three cap proteins constitute the pore region, which represents the wider opening of the RNA entrance funnel. The narrowest point of this funnel marks the neck region that is formed at the top of the Rrp41-Rrp42 hexameric barrel (Fig. 1a)13–15.

The Rrp4 protein, encoded side by side with the core proteins Rrp41 and Rrp42 in a highly conserved archaeal superoperon19, is composed of an N-terminal, an S1 and a KH domain (Fig. 1a). The trimeric Rrp4 cap structure increases the catalytic efficiency of the enzyme complex7,16.and provides substrate specificity for polyadenine (polyA) or adenine-rich stretches of RNA8,16. Interestingly, the rate at which the Rrp4-exosome complex degrades its substrate depends on the remaining length of the RNA substrate. For long RNA substrates the degradation efficiency is constant from the 3’-end to nucleotide 24, then the degradation rate increases between nucleotides 24 and 14 after which the efficiency rapidly drops17,20. These variations in degradation speed were observed for polyA RNA and are thus caused by the degradation mechanism of the enzyme and not by the RNA sequence or its structural features. The mechanism that underlies this variation in degradation rate and the way RNA interacts with the Rrp4 cap structure remains elusive.

NMR spectroscopy is a powerful tool to study biomolecular interactions21 as it can provide quantitative information regarding which residues participate in the interaction. In combination with methyl group labeling22,23 and TROSY techniques24, interaction information can be extracted for complexes that are over 100 kDa25–27 and in some cases even up to 1 MDa28. One drawback of methyl TROSY NMR spectroscopy is that parts of interaction interfaces can be devoid of methyl groups, which renders these surfaces invisible for the experiment and thereby limits the binding-site mapping precision. Recently, this limitation was overcome with methionine scanning, a method where reporter methionine residues are introduced into the protein at a location of interest29,30. In addition to identifying the binding interface with per residue resolution, methionine scanning allows to determine hot-spot positions that are essential for the interaction30.

Here, we study the *Sulfolobus solfataricus* archaeal Rrp4-exosome in complex with substrate RNA (~300 kDa) using methyl TROSY NMR spectroscopy. We found three 50 Å long binding channels in Rrp4 that span all domains of the cap complex and we localized hot-spot positions in Rrp4 and in the exosome core. Using affinity measurements we show that the local interaction strength between the substrate and the enzyme increases in a stepwise manner from the periphery of the cap structure towards the pore region, the neck region and the region at the active sites inside the core complex. Our data show that while one substrate molecule enters the enzyme through the neck, two additional substrate molecules can be

positioned on the cap structure awaiting degradation. Interestingly, we find that the binding energy between Rrp4 cap and the substrate is substantially reduced after the 3' end of the RNA enters the catalytic barrel, thereby reducing friction during the degradation of the substrate.

Results

NMR spectra of the 270 kDa complex are of high quality

The 270 kDa Rrp4-exosome complex is among the largest complexes studied using high-resolution NMR spectroscopy31. To simplify the NMR spectra, we labeled only the Rrp4 subunits with NMR active methyl groups (see Methods). Using methyl TROSY NMR techniques24, we were able to record high quality spectra to study the interaction between the Rrp4 cap and RNA substrate (Fig. 1b). The isoleucine and methionine resonances were assigned by a combination of the "divide and conquer"28 and mutagenesis approaches32,33 (Supplementary Results, Supplementary Fig. 1). With these methods we assigned 69% of all NMR active methyl group resonances in our spectra.

To address which residues in Rrp4 play a role in the substrate–enzyme interactions we added three equivalents of an RNA substrate (see methods) to the Rrp4-exosome complex, which resulted in a large number of chemical shift perturbations (CSPs) (Fig. 1b). Based on the assignments of the methyl groups, we conclude that the Rrp4 S1 (pore region) and KH (periphery) domains are most prominently involved in RNA interactions. The number and location of residues that undergo CSPs show that the large area of the Rrp4 surface is used for the interaction with RNA substrate (Fig. 1).

Increasing the coverage of methyl groups on the surface

The naturally occurring methyl groups are only sparsely distributed over the surface of the Rrp4 complex (Supplementary Fig. 2). Methyl TROSY spectroscopy is thus "blind" for most of the surface of the cap structure and as a result these regions cannot provide information regarding intermolecular interactions. We made those invisible areas on the surface visible using methionine scanning30, where we replaced residues at the surface, one at a time, with reporter methionine residues. These methionine residues then directly report on binding events at the specific location on the surface (Fig. 2). One substantial advantage of methionine scanning is that the introduced methyl group appears as a novel resonance in the spectrum and can thus be assigned instantaneously. To improve the spectral quality and to prevent signal overlap in the methionine region, we mutated three natural methionine residues in the flexible and unstructured N-terminal region of Rrp4 to serine residues, which did not interfere with the structure and activity of the enzyme (Supplementary Fig. 3a).

In total, we selected 30 residues on the Rrp4 surface and substituted them with reporter methionine residues (Supplementary Table 1). 28 of these reporter methionine residues gave rise to a readily identifiable single resonance in the corresponding methyl TROSY NMR spectrum, without interfering with the integrity of the enzyme complex (Supplementary Fig. 3b,c). To each of these samples we added a three-fold molar excess of RNA to probe for binding at the site of the reporter methionine. In brief, we observed 3 different scenarios.

First: the introduced reporter methionine is unaffected by the addition of the RNA (Supplementary Fig. 4), while the naturally occurring isoleucine residues show the same CSPs as we observed for the WT complex. These positions are therefore considered to be outside the RNA binding site. Second: the reporter methionine shows a CSP upon addition of the substrate, proving that this residue is inside the RNA binding site. We find these residues in the KH domain of Rrp4 and close to the RNA entrance pore. Depending on the chemical shift differences between the free and RNA-bound state of the Rrp4-exosome, the CSPs are visible as a shift (Fig. 2a, Supplementary Fig. 5) or a splitting (Fig. 2b, Supplementary Fig. 6a, b) of methyl group resonance frequencies. It is important to note that signals that split titrate to the RNA bound state upon addition of an excess of RNA. This indicates that the exosome cap structure is symmetric in the fully RNA bound state (see below). Lastly, we observed a scenario where the reporter methionine resonance is unaffected by the substrate RNA while the naturally occurring isoleucine residues display substantially reduced CSPs (Fig. 2c). In this case, we identified a hot-spot residue that, when mutated, interferes with substrate binding (Fig. 2c, Supplementary Fig. 7a). The identified hot-spot is in the GKNK loop of the KH domain, which is at the periphery of the cap structure. This confirms previous reports that mutations in this loop of a KH domain abolish RNA binding, without influencing the structure34. Importantly, this hot-spot in Rrp4 only abolishes RNA interactions at the periphery of the complex as interactions between the residues in the pore region and RNA are unaffected (Supplementary Fig. 7b). The hot-spot we identified thus only locally interferes with the RNA interaction and does not affect cap–RNA interactions in other areas. This shows that the S1 and KH domains in Rrp4 interact with RNA independently, which is in agreement with findings for the *Arabidopsis thaliana* Rrp4 protein35.

Hot-spots have a functional role in RNA degradation

To address the functional role of the local hot-spot that we identified in the Rrp4 cap structure and to identify additional critical residues in this region we performed RNA degradation experiments (methods, Fig. 3a)18. In agreement with previous reports7,16, the presence of the Rrp4 cap proteins increases the catalytic efficiency of the exosome (Fig. 3a). However, in case the exosome core was in complex with the Rrp4 protein that contains mutations in a hot-spot location, this increase in catalytic efficiency was no longer observed (Fig. 3a). This indicates that the hot-spot that we identified plays an important role in the RNA degradation process. Based on RNA degradation experiments combined with NMR binding experiments we identified additional hot-spot residues that clustered around the interface between the KH domain and the NTD (Fig. 3a, b). Importantly, all of these mutants are properly folded and interact normally with the exosome core (Supplementary Fig. 7b). It is unlikely that the hot-spot mutations in Rrp4 influence the active sites in the exosome core through an allosteric mechanism as addition of the Rrp4 cap to the exosome core does perturb the resonances close to the active sites25. Rather, we postulate that the periphery of the Rrp4-exosome complex plays a role in the first contacts between the enzyme and the RNA substrate. Mutations in this region are thus likely to interfere with the RNA recognition and recruitment process.

The narrowest point of the RNA funnel, the neck, is formed by the Rrp41 and Rrp42 proteins and is located just below the Rrp4 pore (Fig. 1a). Mutations that invert the positive charge in this region have been reported to block RNA degradation for the *Archaeoglobus fulgidus* exosome16. Here, we show that the equivalent mutation (Rrp41 R67E) in the neck region abolishes the activity of the *Sulfolobus solfataricus* core exosome (Fig. 3a). Interestingly, the activity of this mutated exosome core can be rescued by the Rrp4 cap (Fig. 3a). This indicates that the inactivity of the neck mutant is due to impairments in the RNA interaction (see below) and not due to blocking of the entrance to the catalytic chamber of the core. In the neck mutation background (Rrp41 R67E), the Rrp4 cap provides RNA binding sites that can then funnel the RNA to the active sites. These findings underscore the importance of the Rrp4 cap in the substrate RNA recognition process.

RNA interacts over a long stretch of the cap surface

Our NMR data (Fig. 1, 2), together with the RNA degradation assays (Fig. 3a), reveal that the substrate RNA interacts with Rrp4 surface over a long binding path (Fig. 3b). This path starts on the periphery of the complex, around the identified hot-spots and runs over 50 Å through the KH-NTD groove and into the S1 pore to the neck of the core exosome. The Rrp4 cap thus funnels the substrate through the neck region towards the active sites.

To structurally validate the binding path we identified here, we compared the RNA binding sites in the NTD, S1 and KH domains with known protein–RNA structures (Supplementary Fig. 8). To that end, we performed DALI searches36 with the Rrp4 domains and selected structures that contain RNA. We observe that the binding sites of the Rrp4 KH and S1 domains are compatible with known complex structures. Interestingly, the affected residues we identified in the Rrp4 NTD do not correspond to residues that were reported to be involved in RNA recognition in this domain (Supplementary Fig. 8) and thus represent a novel RNA biding site.

The energetics of the exosome–RNA interaction

To address the overall affinity of the exosome for the RNA substrate we used fluorescence anisotropy measurements. For the interaction between the Rrp4-exosome complex and RNA, we extracted an affinity of 67.5 ± 22.7 nM (Fig. 4a; Supplementary Table 2, complex B), which corresponds to a binding Gibbs free energy (ΔG^0) of –9.97 ± 0.20 kcal/mol ($\Delta G = -RT\ln(K_D)$; T= 30 °C).

Based on known crystal structures15, our previous NMR experiments18 and our methionine scanning data (Fig. 2, 3b), there are four regions in the Rrp4-exosome complex that can interact with the RNA: the active sites and the neck region in the hexameric exosome core15,18 in addition to the pore and periphery regions in the Rrp4 cap structure (Fig. 3b). To dissect the energetic contribution of each of these regions to the overall affinity between the Rrp4-exosome and substrate RNA we used Rrp4-exosome versions, where individual RNA–enzyme contact points were abolished. The periphery interaction in Rrp4 was disrupted using the KNK170ENQ mutation (Fig 3a), the cap interaction was removed by using the isolated exosome core, while the neck interaction was disrupted using the R67G18 or the R67E (Fig. 3a) mutation in the core protein Rrp41. In addition, we prevented

interactions between the active sites in the exosome core and the substrate by using a shorter RNA that cannot reach from the neck region to the active sites. For all complexes we quantified the affinity for the RNA substrate using fluorescence anisotropy titrations (Fig. 4a; Supplementary Table 2). Differences in RNA affinity between these complexes provide insights into local intrinsic binding energies for each contact point ($\Delta G^{i}_{A} = \Delta G^{0}_{ABCD} - \Delta G^{0}_{BCD}$; where A to D are the four contact points)37. As an example, the Rrp4 contribution (ΔG^{i}_{Rrp4}) to the overall affinity between the Rrp4-exosome complex and the RNA can be extracted by comparing the RNA affinity of the Rrp4-exosome complex ($\Delta G^{0}_{Rrp4\text{-}exosome}$; Supplementary Table 2, complex B) with that of the isolated exosome core (ΔG^{0}_{Core}; Supplementary Table 2, complex A). This contribution of the Rrp4 cap to the RNA binding energy can be extracted independently based on different versions of the exosome core (e.g. with the mutation R67G in Rrp41), with and without the cap proteins (Supplementary Table 2, complexes E and F). Taken together, we were able to extract the intrinsic binding energies for all four RNA contact points in a number of independent ways (Fig. 4b; Supplementary Table 3).

In summary, our data show that the local intrinsic binding energies between the substrate and the exosome complex increase from the periphery of the complex towards the active sites (Fig. 4b, left). The fact that the highest energy contribution resides at the active sites assures that the substrate efficiently ratchets one base further after catalysis. Interestingly, the intrinsic binding energy of the cap is very small, indicating that Rrp4 provides only a limited energetic contribution to the enzyme–substrate interaction. This likely reflects the high entropic cost that is involved in the interaction between the highly flexible RNA substrate and the cap surface38, which prevents a large additive effect of the cap–RNA interaction to the overall binding energy. As a result the 5’ end of the RNA can temporarily dissociate from the Rrp4 cap structure, while the 3’ end remains tightly associated with the core of the exosome complex. It is important to note that the RNA–Rrp4 interactions are nevertheless functionally relevant, as mutations in the periphery of the complex influence the catalytic turnover rates (Fig. 3a).

The exosome recruits three RNA substrates simultaneously

Due to the trimeric nature of the Rrp4 cap structure, three RNA species can interact simultaneously with the exosome complex. The exosome neck is, however, only large enough to accommodate a single RNA substrate that can then interact tightly with the enzyme through all four contact points. The two successive RNA molecules that can be recruited by the cap surface only interact with two Rrp4 contact points: the pore and periphery regions (Figs. 3b, 4b). To experimentally validate the stoichiometry of the RNA-exosome complex, we added a large excess of substrate to the Rrp4-exosome and recorded NMR spectra of the saturated enzyme. We then removed weakly bound RNA substrates from the Rrp4 surface by size exclusion chromatography. NMR spectra of this sample showed that a large fraction of the RNA dissociated from the complex (Supplementary Fig. 9). This supports the notion that one RNA molecule is bound considerably stronger to the Rrp4-exosome complex than the two other substrate molecules. Our data thus reveal that the Rrp4 cap can recruit three substrates simultaneously to the enzyme complex. This is in

agreement with previous findings that show that Rrp4 can enhance the substrate recruitment to the exosome17.

In our fluorescence anisotropy measurements the two weaker binding events remain invisible, as the exosome concentration is in excess of the RNA concentration and all RNA molecules are recruited to the strongest exosome interaction site. To obtain insights into the interaction of the two additional RNA substrates with the Rrp4 cap, we made use of NMR titration experiments, where excess RNA will occupy weaker binding site. We exploited the Rrp4 I85M methionine reporter mutant (see above), as it is located deep inside the Rrp4 pore (Supplementary Table 1). During 16 titration steps, we added RNA substrate to the Rrp4-exosome complex and monitored the induced CSPs (Fig 1, Fig 4c and Supplementary Figs. 10-12). To determine the RNA–Rrp4 cap affinity we then analyzed the NMR line-shapes during the titration experiments for 8 different resonances. The fitting of NMR line-shapes to specific binding models has proven to be an accurate method to extract kinetic parameters39–41. Here, we used a model for the interaction between three RNA substrates and the Rrp4 exosome that takes into account that the NMR line-shapes are a superposition of the first RNA binding event (with an overall affinity in the high nM range; Supplementary Table 2) and the two subsequent weaker binding events. In addition, we included the fact that the 5’ end of the RNA that contacts the exosome core can temporarily dissociate from Rrp4 due to the small intrinsic binding energy with the cap (Supplementary Table 3; see above; Supplementary Figs. 10, 11). Based on the binding model we optimized the kinetic parameters to minimize the square of the difference between the experimental NMR spectra and the NMR spectra that were simulated based on the binding model (Fig. 4c, Supplementary Figs. 12, 13).

From the global fit we extracted that the RNA interacts with the Rrp4 cap with a K_D of 20.4 ± 2.1 μM (Fig. 4c; Supplementary Table 2, complex K), which corresponds to a free energy of binding of –6.50 ± 0.06 kcal/mole (Fig. 4b). From that we conclude that two additional RNAs are recruited to the cap in the Rrp4-exosome complex with μM affinity.

We then repeated the NMR titration experiments using the Rrp4-exosome complex where mutations in the periphery of the cap structure prevent RNA binding in this region. In that case, the affinity between the exosome and the second and third RNA is reduced to 60.5 ± 5.1 μM, corresponding to a free energy of –5.85 ± 0.04 kcal/mole (Supplementary Fig. 14; Supplementary Table 2, complex L). This confirms that the intrinsic binding energy of the periphery region is small (Supplementary Table 3) despite its functional significance (Fig. 3a).

Discussion

Static high-resolution structures are indispensible for understanding the mechanism of molecular machines. These structures, however, hide dynamic features that are important for biological function. Here, we address how the Rrp4-exosome complex recruits substrate RNA molecules and how the enzyme is able to channel these towards the active sites.

Using methyl TROSY NMR spectroscopy and degradation assays we identified a 50 Å long RNA interaction channel that covers a large portion of the Rrp4 surface between the periphery and the RNA entrance pore (Fig. 3, 5). This path is in agreement with a very low resolution SAXS reconstruction of the *Archaeoglobus fulgidus* Rrp4-exosome in complex with RNA 17, where the RNA appears to make contacts with the top of the Rrp4 cap. At the same time, the interactions that we observed on the archaeal cap structure differ from the RNA interactions that have been reported for the eukaryotic exosome cap proteins (Supplementary Fig. 15). Whether these differences are due to variations in the substrate recruitment mechanism, the RNA used in the experiment or the complex composition (e.g. the presence of Rrp6 in the eukaryotic exosome)10,11,42 remains to be determined.

Although the large RNA interaction surface on the Rrp4 protein in the archaeal exosome is advantageous for substrate recruitment (Fig. 5), it can potentially compromise catalysis as excessive friction would hamper motions of the RNA towards the active sites 17. Optimal catalytic efficiency is thus a trade-off between efficient substrate recruitment and rapid substrate translocation. Our binding experiments show that Rrp4 can recruit RNA substrates with μM affinity. This RNA is initially in contact with both the periphery and the pore of the Rrp4 cap structure complex. When the entrance pore is free, the 3’ end of the substrate can move into the core, such that it contacts all four interaction sites (periphery, pore, neck and active sites; Fig. 4b,5). This step will be driven by a significant change in binding free energy from –6.50 kcal/mol (μM affinity) to –9.97 kcal/mol (nM affinity) (Supplementary Table 2, Fig. 4b).

After the substrate is fully bound to the enzyme, the 3’ terminal nucleotide can be phosphorolyzed at the active sites. This will result in a release of a nucleotide diphosphate product and a loss of the interactions between the substrate and the active sites. Subsequently, the RNA will ratchet one base further such that the new 3’ end can engage in interactions with the active sites. This movement will result in a favorable change of the binding free energy between the enzyme and the substrate of up to –3.15 kcal/mol (Fig 4, Supplementary Table 2). This change in free energy is much smaller than was previously calculated for the eukaryotic complex43, where RNA degradation takes place in the additional exosome component Rrp44. This difference correlates well with the fact that the eukaryotic exosome, unlike the archaeal exosome, is able to process RNA substrates that contain secondary structure elements that need to unfold before entering into the exosome barrel.

The combination of the four independent interaction points is able to explain the molecular basis for the dependence of the degradation velocity on substrate length17,20. Substrates longer than 24 nucleotides will interact with the enzyme through all sites (periphery, pore, neck and active sites). For substrates shorter than 24 nucleotides, the RNA is too short to reach from the active site to the periphery and the friction between the RNA and the Rrp4 cap is reduced, which results in an increase in degradation velocity17. For substrates shorter than 13 nucleotides the RNA is too short to interact simultaneously with the active sites and the neck region. This releases the RNA from the pivotal point in the neck of the exosome complex18 and results in a decrease of the degradation rate, as the substrate is no longer tightly restrained to the barrel of the complex17.

It is important to note that the ΔG^{i} values appear more negative when the two binding sites influence each other in a constructive manner and appear less negative when the two binding events influence each other negatively (see Supplementary Fig. 16). Interestingly, our data displays a situation where the sum of the four individual intrinsic binding energies (ΔG^{i}) is smaller than the overall binding energy ($\Delta G^{0}_{\text{Rrp4-exosome}}$). Assuming that there are no additional interaction sites between the substrate and the enzyme, this displays two important features of the RNA–enzyme interaction. First, there is no additivity in the multivalent RNA–exosome binding processes37,44. The lack of additive binding effects has also been observed e.g. for the interaction between the tau protein and microtubules45 and for the interaction between the trigger factor chaperone and the unfolded alkaline phosphatase substrate46. In those examples, and in the case of the flexible RNA we study here, the interaction with one binding site is unable to position other motifs in the proper binding position and at each interaction site a large entropic cost has to be paid. Second, the small sum of the intrinsic binding energies suggests that the RNA backbone adopts an energetically unfavorable conformation upon interaction with the enzyme, which is plausible, as the RNA must make a tight turn upon entering the barrel of the Rrp4-exosome complex. Mechanistically this has important advantages for the degradation process. In particular, the initial recruitment of the substrate by the Rrp4 cap involves a binding energy of ΔG = –6.50 kcal/mol (Supplementary Table 2). This energy would invoke substantial friction between the substrate and the enzyme such that degradation rates would be substantially reduced. However, upon translocation of the 3’ end of the RNA substrate into the exosome core (which is driven by an increase in the binding free energy of –3.47 kcal/mol; Supplementary Table 2, complex K vs. complex B) the Rrp4–RNA binding energy is substantially reduced to an intrinsic binding energy of around –1 kcal/mol (Supplementary Table 3). The binding groove that recruits substrates does therefore not add substantially to the enzyme–RNA interaction during degradation. The Rrp4-exosome complex can thus combine efficient substrate recruitment without compromising the movement of the substrate towards the active sites (Fig. 5).

In summary, we here reveal a unique mechanism by which the exosome ensures efficient recruitment and motion of the RNA substrate. Our data thus enhance our understanding of the exosome complex and reveal functionally important molecular details that are hidden in static crystal structures. Future work will disclose if the mechanisms that we identified here are general principles that are also exploited by other complex molecular machines.

Online Methods

Protein production

The *Sulfolobus solfataricus* Rrp41-Rrp42 exosome core was obtained by co-expression of the two proteins in LB medium using BL21 (DE3) RIL *E. coli* cells (Stratagene). The core complex was purified using Ni-affinity chromatography and gel filtration as previously described 25. The *Sulfolobus solfataricus* Rrp4 exosome cap protein was obtained by over-expression in D_2O-based minimal medium in the presence of $^{2}H^{12}C$ glucose. Methionine (^{1}H-^{13}C; 100 mg/l) and α-ketobuteric acid (4-$^{1}H_3$-^{13}C, 3-$^{12}C^{2}H_2$; 60 mg/l) were added to the growth medium one hour prior to the induction of protein expression to ensure that the

methyl groups in methionine and isoleucine (δ1) residues are NMR active. Cells were lysed in buffer A (50 mM $NaPO_4$ pH 7.5, 150 mM NaCl, 10 mM Imidazol, 1mM DTT) and Rrp4 was bound to Ni-NTA resin. The resin was washed extensively using buffer A. Subsequently, the exosome core complex was added to the Ni-resin to allow for the formation of the Rrp4-exosome complex during 2 hours at 4 °C with constant tilting. In this way we ensure an equimolar composition of the complex (Supplementary Fig. 17). The reconstituted complex was eluted using buffer A plus 330 mM imidazole. The complex was dialysed into buffer A without imidazole and simultaneously the affinity tag was removed using TEV protease. Subsequently the complex was incubated at 50 °C for 2h and purified to homogeneity using gel filtration in GF buffer (30 mM KPO_4 pH 7, 100 mM NaCl) (Supplementary Fig. 17). It is worth mentioning that the Rrp4 protein could be purified in isolation at low concentration, but that it was not possible to record high quality NMR spectra on the isolated protein.

RNA production

The RNA substrate for NMR experiments was prepared using *in vitro* transcription. The RNA substrate contained a 5’ GC-based hairpin structure followed by 32 adenines (5’-GCCCCCCCCGAAAGGGGGGGAAAAAAAAAAAAAAAAAAAAAAAAAAA-2’-3’ cyclic phosphate). We used a PolyA sequence as this has been shown to be the preferred substrate for the Rrp4-exosome. Based on crystal structures of the Rrp4-exosome complex, the adenine tail is substantially longer than the distance from the Rrp4 periphery to the active sites of the exosome. A homogenous 3’ end of the transcript was ensured by HDV ribozyme cleavage. This resulted in a 2’-3’ cyclic phosphate that also prevented the degradation of the RNA substrate by the exosome complex. The 5’ hairpin structure prevents potential binding of the single stranded substrate RNA in the reverse direction. For degradation experiments, the same RNA was prepared using run-off transcription that results in an RNA that contains a 3’ hydroxyl group, which is an ideal substrate for the exosome complex. This RNA contained three extra bases at the 3’ end that resulted from the linearization of the DNA template (5’-GCCCCCCCCGAAAGGGGGGGAAAAAAAAAAAAAAAAAAAAAAAAAAAAGCU-3’). The RNAs that were used for binding experiments contained a single 4-thiouridine (4-S-U) (long RNA: 5’-GCCCCCCCCGAAAGGGGGGGAAAAAAAAAAAAAAAAAAA-4-S-U-AAAAAAAAAAAGCU-3’, short RNA: 5’-4-S-U-GCCCCCCCCGAAAGGGGGGGAAAA) and were obtained from Dharmacon.

NMR Spectroscopy

NMR spectra were recorded at 50 °C on an AVIII-800 spectrometer with room temperature probe-heads. HMQC methyl TROSY spectra were recorded with a carbon acquisition time of 45 ms. Spectra were processed using the NMRPipe/NMRDraw software suite47, using zero-filling to 2k (1k) points in the direct (indirect) dimension to increase digital resolution. For NMR titration experiments, the substrate RNA was added to a 15.75-fold molar excess (RNA concentration over the concentration of the full exosome complex) in 15 steps. For methionine scanning experiments RNA was added to an approximately 3:1 ratio. Small differences in the RNA: protein ratio in the methionine scanning spectra result in differences

in the saturation of the Rrp4-exosome with RNA. This does not influence the interpretation of the methionine scanning data, that only determine if a residue is outside or inside the RNA interaction groove or if the residue interferes with RNA binding.

NMR methyl groups of isoleucine residues were assigned based on the “divide and conquer” approach, where parts of the large complex are assigned in isolation followed by the transfer of these assignments to the intact complex. The 28 kDa full-length Rrp4 protein is not stable without the exosome core complex, but we found that a truncated form of Rrp4 that only contains the S1 and KH domains can be purified. Methyl group assignments of this monomeric 21 kDa Rrp4 fragment were obtained using traditional TROSY based methods48 and could be partially transferred to the 270 kDa Rrp4-exosome complex (Supplementary Fig. 1a). The methyl group assignments that were obtained in this step were complemented with a number of assignment mutants32,33 (Supplementary Table 1). In that case, single isoleucine or methionine methyl groups were replaced with an alternative amino acid, which ideally results in the disappearance of a single resonance from the methyl TROSY NMR spectrum (Supplementary Fig. 1b).

To extract the binding constant for the interaction between the RNA and the exosome cap one-dimensional traces were extracted from the two-dimensional spectra using the nmrPipe/nmrDraw software suite47. These 1D spectra were fitted using numerical equations for NMR resonance lines taking into account the model that is described in detail in Supplementary Fig. 10-13. Errors in the determined parameters were obtained through a Jackknife approach, where single residues were omitted from the fitting procedure. Details of the fitting procedure and of the used model are described in Supplementary Fig. 10 and 11.

Fluorescence Anisotropy

For fluorescence anisotropy measurements, the substrate RNA containing a 4-thiouridine was coupled to 6-(Iodoacetamido)-fluorescein49. RNA (10 nM) was mixed with increasing amounts of several variants of the exosome (0 to 2000 nM or 0 to 80 μM full exosome complex, depending on the affinity) in 96 well plates. After 2h incubation changes in fluorescence anisotropy were detected using a plate reader (Tecan, Infinite F200; filter linear polarization XP38; excitation at 485 nm and emission at 535 nm). Binding curves were fitted to the standard equation for a one-site binding model50 using in house written scripts. Errors in the measurements were extracted from fully independent measurements as indicated in the legend of Supplementary Table 2.

Degradation assay, HPLC

RNA degradation experiments were performed by mixing RNA substrate (25 μM) with different versions of the exosome complex (60 nM exosome) in 180 μl reaction buffer (20 mM Hepes pH 6.5, 60 mM KCl, 0.1 mM EDTA, 2 mM DTT, 8 mM $MgCl_2$, 10 mM Na_2HPO_4) at 50 °C. 10 μl aliquots of the reaction mix were taken at 12 different defined time-points and the reaction was quenched by mixing the aliquots 1:1 with 8 M Urea, 20 mM EDTA, 2 mM Tris pH 8. The amounts of substrate and product (a 5’ GC based hairpin structure followed by 10 adenines) were quantified on a DNAPac PA100 column (Dionex)

using a linear gradient from buffer A (5 M Urea, 20 mM Tris pH 8, 100 mM NaCl) to buffer B (5 M Urea, 20 mM Tris pH 8, 2 M NaCl). Peak intensities were translated into concentrations from which the turnover numbers were extracted by linear fitting of the 12 timepoints18.

Data availability

All data generated or analyzed during this study are included in this published article (and its supplementary information files) or are available from the corresponding author upon reasonable request.

Supplementary Material

Refer to Web version on PubMed Central for supplementary material.

Acknowledgements

We acknowledge all members of the laboratory for discussions. We thank Silke Wiesner for suggestions regarding the methionine scanning experiments, Iris Holdermann and Janina Petters for excellent technical assistance and Vincent Truffault for maintenance of the NMR infrastructure. M.A.C. and S.S. acknowledge funding from the IMPRS “From Molecules to Organisms”. This work was supported by the Max Planck Society and the European Research Council under the European Union’s Seventh Framework Programme (FP7/2007–2013), ERC grant agreement no. 616052 (R.S.).

References

1. Mitchell P, Petfalski E, Shevchenko A, Mann M, Tollervey D. The exosome: a conserved eukaryotic RNA processing complex containing multiple 3'--> 5' exoribonucleases. Cell. 1997; 91:457–66. [PubMed: 9390555]
2. Bousquet-Antonelli C, Presutti C, Tollervey D. Identification of a regulated pathway for nuclear pre-mRNA turnover. Cell. 2000; 102:765–75. [PubMed: 11030620]
3. Mitchell P, Petfalski E, Tollervey D. The 3' end of yeast 5.8S rRNA is generated by an exonuclease processing mechanism. Genes Dev. 1996; 10:502–13. [PubMed: 8600032]
4. van Hoof A, Frischmeyer PA, Dietz HC, Parker R. Exosome-mediated recognition and degradation of mRNAs lacking a termination codon. Science. 2002; 295:2262–4. [PubMed: 11910110]
5. Dziembowski A, Lorentzen E, Conti E, Seraphin B. A single subunit, Dis3, is essentially responsible for yeast exosome core activity. Nat Struct Mol Biol. 2007; 14:15–22. [PubMed: 17173052]
6. Evguenieva-Hackenberg E, Walter P, Hochleitner E, Lottspeich F, Klug G. An exosome-like complex in Sulfolobus solfataricus. EMBO Rep. 2003; 4:889–93. [PubMed: 12947419]
7. Walter P, et al. Characterization of native and reconstituted exosome complexes from the hyperthermophilic archaeon Sulfolobus solfataricus. Mol Microbiol. 2006; 62:1076–89. [PubMed: 17078816]
8. Roppelt V, Klug G, Evguenieva-Hackenberg E. The evolutionarily conserved subunits Rrp4 and Csl4 confer different substrate specificities to the archaeal exosome. FEBS Lett. 2010; 584:2931–6. [PubMed: 20488184]
9. Wasmuth EV, Januszyk K, Lima CD. Structure of an Rrp6-RNA exosome complex bound to poly(A) RNA. Nature. 2014; 511:435–9. [PubMed: 25043052]
10. Liu Q, Greimann JC, Lima CD. Reconstitution, activities, and structure of the eukaryotic RNA exosome. Cell. 2006; 127:1223–37. [PubMed: 17174896]
11. Makino DL, Baumgartner M, Conti E. Crystal structure of an RNA-bound 11-subunit eukaryotic exosome complex. Nature. 2013; 495:70–5. [PubMed: 23376952]

12. Lorentzen E, et al. The archaeal exosome core is a hexameric ring structure with three catalytic subunits. Nat Struct Mol Biol. 2005; 12:575–81. [PubMed: 15951817]
13. Navarro MV, Oliveira CC, Zanchin NI, Guimaraes BG. Insights into the mechanism of progressive RNA degradation by the archaeal exosome. J Biol Chem. 2008; 283:14120–31. [PubMed: 18353775]
14. Lorentzen E, Conti E. Structural basis of 3' end RNA recognition and exoribonucleolytic cleavage by an exosome RNase PH core. Mol Cell. 2005; 20:473–81. [PubMed: 16285928]
15. Lorentzen E, Dziembowski A, Lindner D, Seraphin B, Conti E. RNA channelling by the archaeal exosome. EMBO Rep. 2007; 8:470–6. [PubMed: 17380186]
16. Buttner K, Wenig K, Hopfner KP. Structural framework for the mechanism of archaeal exosomes in RNA processing. Mol Cell. 2005; 20:461–71. [PubMed: 16285927]
17. Hartung S, Niederberger T, Hartung M, Tresch A, Hopfner KP. Quantitative analysis of processive RNA degradation by the archaeal RNA exosome. Nucleic Acids Res. 2010; 38:5166–76. [PubMed: 20392821]
18. Audin MJ, Wurm JP, Cvetkovic MA, Sprangers R. The oligomeric architecture of the archaeal exosome is important for processive and efficient RNA degradation. Nucleic Acids Res. 2016; 44:2962–73. [PubMed: 26837575]
19. Koonin EV, Wolf YI, Aravind L. Prediction of the archaeal exosome and its connections with the proteasome and the translation and transcription machineries by a comparative-genomic approach. Genome Res. 2001; 11:240–52. [PubMed: 11157787]
20. Niederberger T, Hartung S, Hopfner KP, Tresch A. Processive RNA decay by the exosome: merits of a quantitative Bayesian sampling approach. RNA Biol. 2011; 8:55–60. [PubMed: 21282980]
21. Wiesner S, Sprangers R. Methyl groups as NMR probes for biomolecular interactions. Curr Opin Struct Biol. 2015; 35:60–67. [PubMed: 26407236]
22. Kerfah R, Plevin MJ, Sounier R, Gans P, Boisbouvier J. Methyl-specific isotopic labeling: a molecular tool box for solution NMR studies of large proteins. Curr Opin Struct Biol. 2015; 32:113–22. [PubMed: 25881211]
23. Gardner KH, Kay LE. Production and incorporation of N-15, C-13, H-2 (H-1-delta 1 methyl) isoleucine into proteins for multidimensional NMR studies. Journal of the American Chemical Society. 1997; 119:7599–7600.
24. Tugarinov V, Hwang PM, Ollerenshaw JE, Kay LE. Cross-correlated relaxation enhanced 1H[bond]13C NMR spectroscopy of methyl groups in very high molecular weight proteins and protein complexes. J Am Chem Soc. 2003; 125:10420–8. [PubMed: 12926967]
25. Audin MJ, et al. The archaeal exosome: identification and quantification of site-specific motions that correlate with cap and RNA binding. Angew Chem Int Ed Engl. 2013; 52:8312–6. [PubMed: 23804404]
26. Gelis I, et al. Structural basis for signal-sequence recognition by the translocase motor SecA as determined by NMR. Cell. 2007; 131:756–69. [PubMed: 18022369]
27. Rosenzweig R, Moradi S, Zarrine-Afsar A, Glover JR, Kay LE. Unraveling the mechanism of protein disaggregation through a ClpB-DnaK interaction. Science. 2013; 339:1080–3. [PubMed: 23393091]
28. Sprangers R, Kay LE. Quantitative dynamics and binding studies of the 20S proteasome by NMR. Nature. 2007; 445:618–22. [PubMed: 17237764]
29. Mari S, et al. Structural and functional framework for the autoinhibition of Nedd4-family ubiquitin ligases. Structure. 2014; 22:1639–49. [PubMed: 25438670]
30. Stoffregen MC, Schwer MM, Renschler FA, Wiesner S. Methionine scanning as an NMR tool for detecting and analyzing biomolecular interaction surfaces. Structure. 2012; 20:573–81. [PubMed: 22483105]
31. Rosenzweig R, Kay LE. Bringing dynamic molecular machines into focus by methyl-TROSY NMR. Annu Rev Biochem. 2014; 83:291–315. [PubMed: 24905784]
32. Sprangers R, Gribun A, Hwang PM, Houry WA, Kay LE. Quantitative NMR spectroscopy of supramolecular complexes: dynamic side pores in ClpP are important for product release. Proc Natl Acad Sci U S A. 2005; 102:16678–83. [PubMed: 16263929]

33. Amero C, et al. A systematic mutagenesis-driven strategy for site-resolved NMR studies of supramolecular assemblies. J Biomol NMR. 2011; 50:229–36. [PubMed: 21626214]
34. Hollingworth D, et al. KH domains with impaired nucleic acid binding as a tool for functional analysis. Nucleic Acids Res. 2012; 40:6873–86. [PubMed: 22547390]
35. Chekanova JA, Dutko JA, Mian IS, Belostotsky DA. Arabidopsis thaliana exosome subunit AtRrp4p is a hydrolytic 3'-->5' exonuclease containing S1 and KH RNA-binding domains. Nucleic Acids Res. 2002; 30:695–700. [PubMed: 11809881]
36. Holm L, Rosenstrom P. Dali server: conservation mapping in 3D. Nucleic Acids Res. 2010; 38:W545–9. [PubMed: 20457744]
37. Jencks WP. On the attribution and additivity of binding energies. Proc Natl Acad Sci U S A. 1981; 78:4046–50. [PubMed: 16593049]
38. Searle MS, Williams DH. On the stability of nucleic acid structures in solution: enthalpy-entropy compensations, internal rotations and reversibility. Nucleic Acids Res. 1993; 21:2051–6. [PubMed: 7684832]
39. Waudby CA, Ramos A, Cabrita LD, Christodoulou J. Two-Dimensional NMR Lineshape Analysis. Sci Rep. 2016; 6:24826. [PubMed: 27109776]
40. Kovrigin EL. NMR line shapes and multi-state binding equilibria. J Biomol NMR. 2012; 53:257–70. [PubMed: 22610542]
41. Bain AD, Rex DM, Smith RN. Fitting dynamic NMR lineshapes. Magnetic Resonance in Chemistry. 2001; 39:122–126.
42. Makino DL, et al. RNA degradation paths in a 12-subunit nuclear exosome complex. Nature. 2015; 524:54–8. [PubMed: 26222026]
43. Vukovic L, Chipot C, Makino DL, Conti E, Schulten K. Molecular Mechanism of Processive 3' to 5' RNA Translocation in the Active Subunit of the RNA Exosome Complex. J Am Chem Soc. 2016; 138:4069–78. [PubMed: 26928279]
44. Zhou HX, Gilson MK. Theory of free energy and entropy in noncovalent binding. Chem Rev. 2009; 109:4092–107. [PubMed: 19588959]
45. Butner KA, Kirschner MW. Tau protein binds to microtubules through a flexible array of distributed weak sites. J Cell Biol. 1991; 115:717–30. [PubMed: 1918161]
46. Saio T, Guan X, Rossi P, Economou A, Kalodimos CG. Structural basis for protein antiaggregation activity of the trigger factor chaperone. Science. 2014; 344:1250494. [PubMed: 24812405]
47. Delaglio F, et al. NMRPipe: a multidimensional spectral processing system based on UNIX pipes. J Biomol NMR. 1995; 6:277–93. [PubMed: 8520220]
48. Pervushin K, Riek R, Wider G, Wuthrich K. Attenuated T2 relaxation by mutual cancellation of dipole-dipole coupling and chemical shift anisotropy indicates an avenue to NMR structures of very large biological macromolecules in solution. Proc Natl Acad Sci U S A. 1997; 94:12366–71. [PubMed: 9356455]
49. Ramos A, Varani G. A new method to detect long-range protein-RNA contacts: NMR detection of electron-proton relaxation induced by nitroxide spin-labeled RNA. Journal of the American Chemical Society. 1998; 120:10992–10993.
50. Johnson PE, Tomme P, Joshi MD, McIntosh LP. Interaction of soluble cellooligosaccharides with the N-terminal cellulose-binding domain of Cellulomonas fimi CenC 2. NMR and ultraviolet absorption spectroscopy. Biochemistry. 1996; 35:13895–906. [PubMed: 8909286]

Europe PMC Funders Author Manuscripts

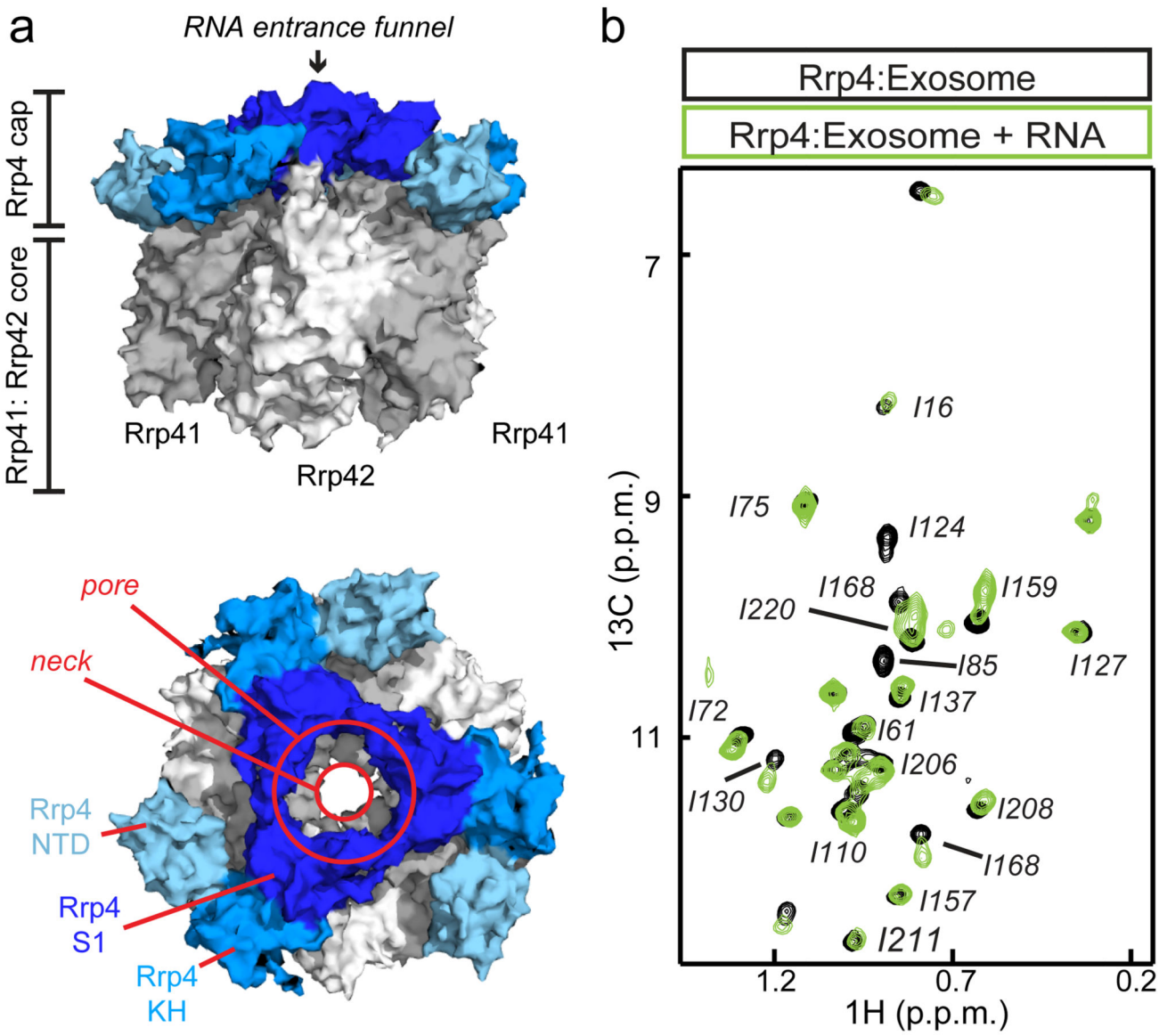

Figure 1. Structure and NMR spectra of the Rrp4-exosome complex.

(a) Side-view (upper panel) and top-view (lower panel) of the *Sulfolobus solfataricus* exosome complex (2JEA 15). Rrp4 subunits are colored in shades of blue (N-terminal domain cyan-blue, S1 domain dark blue, KH domain light blue), the Rrp41 and Rrp42 subunits are colored gray and white respectively. The substrate RNA entrance is indicated, where the Rrp41 subunits determine the narrowest point (the neck region) and the Rrp4 S1 domains form the pore region.

(b) Isoleucine region of the methyl TROSY NMR spectrum of the Rrp4 subunits in the full exosome complex in the absence (black) and presence (green) of RNA substrate. A number of residues experience chemical shift pertubations that report on the RNA–enzyme interaction. Assignments for some resonances are indicated (Supplementary Fig. 1).

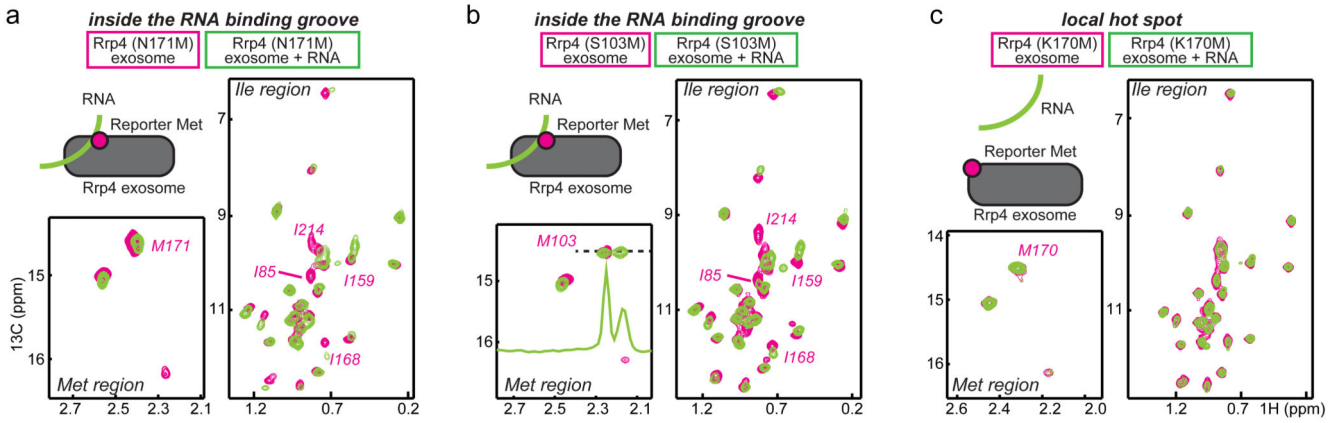

Figure 2. Methionine scanning identifies residues in Rrp4 that interact with substrate RNA.

(a) Spectra of the Rrp4–exosome complex that contain a single introduced reporter methionine (position 171) in the absence (pink) and presence (green) of RNA substrate. The assignment of the reporter methionine is based on the appearance of a novel resonance in the methionine region of the NMR spectra (Supplementary Fig. 4). The N171M reporter mutant shows a CSP upon RNA binding, which places residue 171 in the RNA binding groove. The natural isoleucine residues experience CSPs very similar to the WT situation. This shows that the RNA binds in the same way in the methionine reporter mutant and WT complex.

(b) As in (a), where the signal of the reporter methionine (residue S103) experiences resonance splitting upon addition of one RNA molecule per Rrp4 monomer (Supplementary Fig. 5).

(c) As in (a), where the introduced reporter methionine abolishes RNA binding as indicated by the strong reduction of CSPs of the natural isoleucine residues. Isoleucine residue (I110) that is located in the pore region displays the same CSP as were observed in the WT Rrp4 protein, indicating that the RNA binding is only abolished locally (Supplementary Fig. 6).

Europe PMC Funders Author Manuscripts

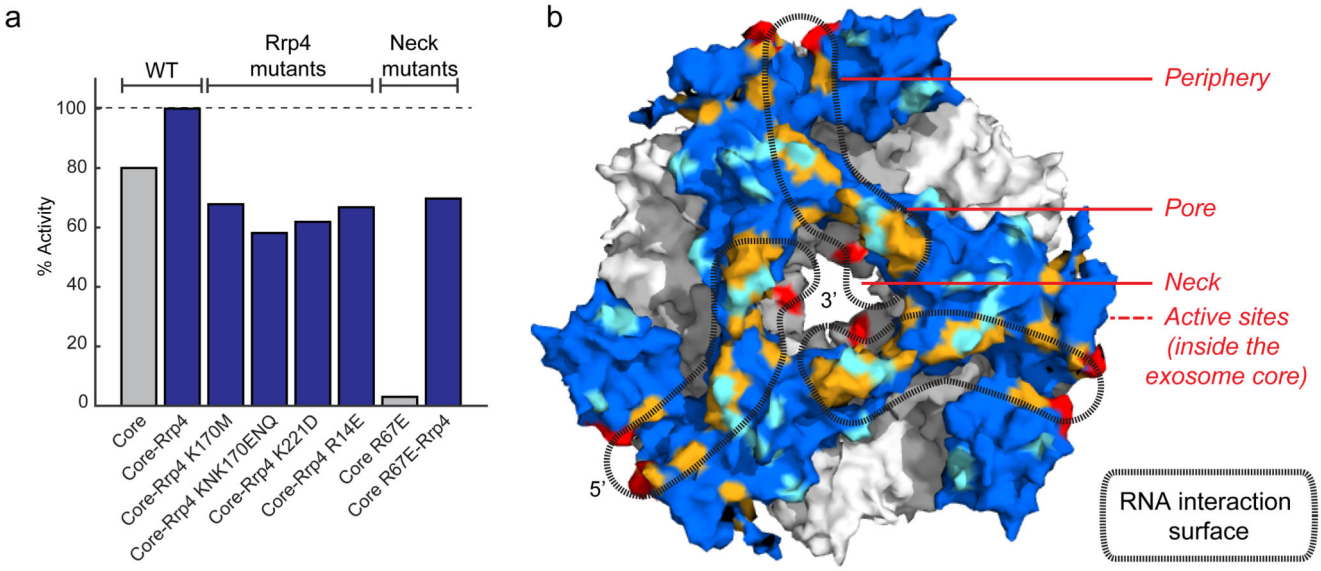

Figure 3. Activity and RNA interaction surface of the Rrp4-exosome

(a) The activity of the exosome complex. Core (grey) refers to the Rrp41–Rrp42 complex; Rrp4-core (blue) refers to the Rrp4-exosome complex. The Rrp4 hot-spot mutants (K170M, KNK170ENQ, K221D and R14E) reduce the catalytic efficiency of the complex. The Rrp41 R67E mutant in the neck of the exosome complex renders the enzyme inactive. This activity can be partially rescued by the addition of the Rrp4 protein. The turnover rates for all complexes were extracted based on degradation series with 12 time points.

(b) Visualization of the NMR binding studies and activity data. The black dashed line indicates the identified surface that is used by Rrp4 to interact with the RNA substrate. Red refers to hot-spot regions, orange to sites that are in contact with the RNA and cyan to sites that are outside the RNA interaction interface. RNA can contact the Rrp4-exosome complex at four different sites: the periphery, the pore, the neck and the active sites (located inside the exosome core).

Europe PMC Funders Author Manuscripts

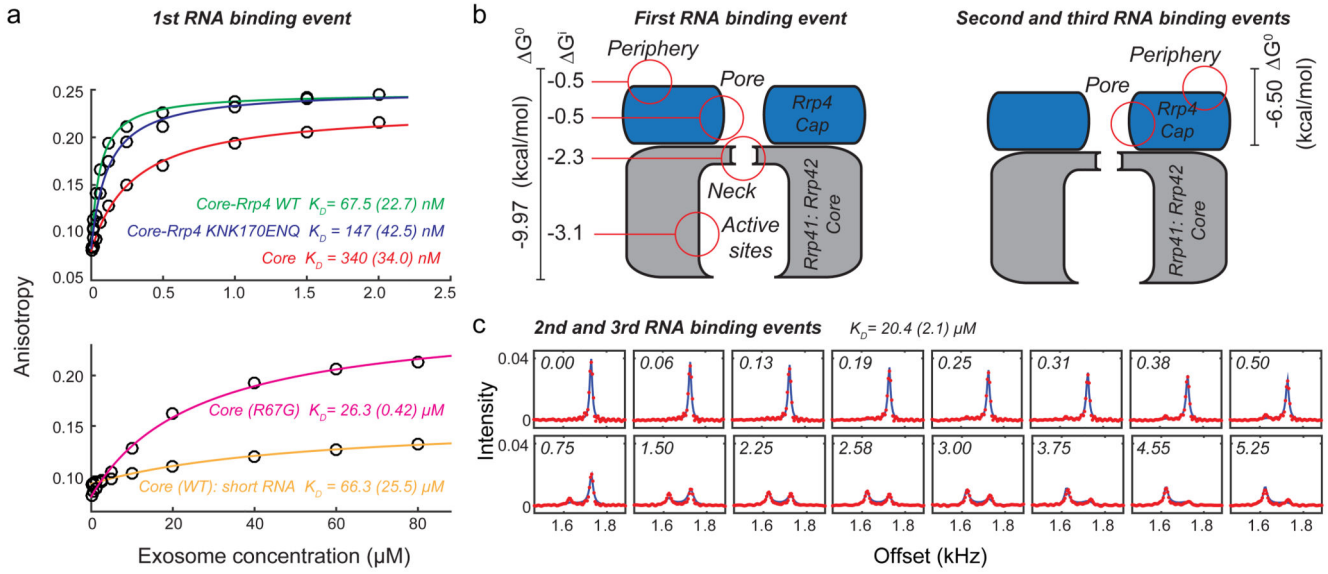

Figure 4. Quantification of the RNA–exosome interactions.

(a) The interaction of the exosome with substrate RNA based on fluorescence anisotropy measurements. The circles represent the experimental data; the solid line is the best fit to the data (Supplementary Table 2). Note that the scale of the x-axis is different in the top and bottom graphs. The indicated errors are derived from independent measurements as indicated in the legend of Supplementary Table 2.

(b) Left: Summary of the binding data for the interaction between the first RNA and the Rrp4-exosome complex. Numbers (Supplementary Table 2) correspond to the interaction of a substrate RNA that is actively degraded. The four interaction sites are indicated. Right: Summary of the interaction between the Rrp4-exosome and the second and third RNA substrate (Supplementary Table 2).

(c) The interaction between the two additional RNA molecules and the Rrp4 protein in the exosome complex is determined based on fitting the NMR titration experiments to a model that describes the interaction between the RNA substrate and the Rrp4-exosome (Supplementary Fig. 10-13). The red dots represent the experimental data, the blue lines result from a global fit of 8 residues that experience CSPs during the NMR titration experiment. For clarity only the data for reporter methionine 85 is shown; data for all fitted residues are presented in Supplementary Fig. 12. The RNA:enzyme ratio is indicated and corresponds to the concentration of the monomeric exosome subunits.

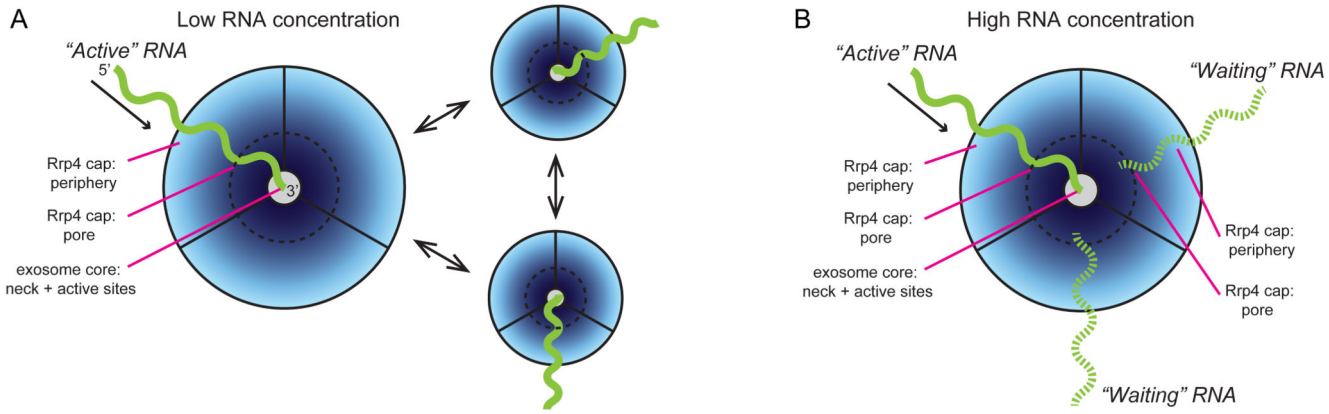

Figure 5. Cartoon of the Rrp4-modulated RNA degradation mechanism.

(a). At low RNA concentration a single RNA is bound to four contact points (active sites, neck, pore and periphery) in the Rrp4 exosome complex. For this RNA, the 5' end is only weakly bound to the Rrp4 cap structure and this part of the substrate can thus temporarily dissociate from the cap and therefore samples all three RNA interaction grooves. The affinity gradient between the RNA and the exosome is depicted using a light- to dark-blue color scheme.

(b). At higher RNA concentration, the Rrp4 cap can recruit two additional substrates with μM affinity. These RNA molecules interact with the complex through contacts with the pore and periphery regions only and are not actively degraded, as only a single RNA substrate is able to pass the neck region. The interaction energy between the cap protein and the substrate is substantially reduced when the 3' end of the RNA moves into the catalytic core, thereby reducing molecular friction that could compromise substrate translocation to the active sites.

Europe PMC Funders Author Manuscripts